







RESEARCH ARTICLE

Age and anatomical region-related differences in vascularization of the porcine meniscus using microcomputed tomography imaging

Ville-Pauli Karjalainen¹  | Valentina R. Herrera Millar² | Silvia Modena³ | Giuseppe M. Peretti^{2,4} | Margherita Pallaoro³ | Khaled Elkhoully¹  | Simo Saarakkala^{1,5}  | Ali Mobasheri¹  | Alessia Di Giancamillo⁴  | Mikko A. J. Finnilä¹ 

¹Research Unit of Health Sciences and Technology, Faculty of Medicine, University of Oulu, Oulu, Finland

²Tissue Engineering and Biomaterials Lab, IRCCS Ospedale Galeazzi Sant'Ambrogio, Milan, Italy

³Department of Veterinary Medicine and Animal Sciences, University of Milan, Milan, Italy

⁴Department of Biomedical Sciences for Health, University of Milan, Milan, Italy

⁵Department of Diagnostic Radiology, Oulu University Hospital, Oulu, Finland

Correspondence

Ville-Pauli Karjalainen, Research Unit of Health Sciences and Technology, Faculty of Medicine, University of Oulu, POB 5000, FI-90014 Oulu, Finland.
Email: ville-pauli.karjalainen@oulu.fi

Funding information

Research Council of Finland (Former Academy of Finland), Grant/Award Number: 353755; Finnish Cultural Foundation, Grant/Award Number: 00220451; Jane ja Aatos Erkko Foundation, Grant/Award Number: 347445; Academy of Finland

Abstract

Meniscal lesions in vascularized regions are known to regenerate while lack of vascular supply leads to poor healing. Here, we developed and validated a novel methodology for three-dimensional structural analysis of meniscal vascular structures with high-resolution microcomputed tomography (μ CT). We collected porcine medial menisci from 10 neonatal (not-developed meniscus, n-) and 10 adults (fully developed meniscus, a-). The menisci were cut into anatomical regions (anterior horn (n-AH and a-AH), central body (n-CB and a-CB), and posterior horn (n-PH and a-PH). Specimens were cut in half, fixed, and one specimen underwent critical point drying and μ CT imaging, while other specimen underwent immunohistochemistry and vascularity biomarker CD31 staining for validation of μ CT. Parameters describing vascular structures were calculated from μ CT. The vascular network in neonatal spread throughout meniscus, while in adult was limited to a few vessels in outer region, mostly on femoral side. n-AH, n-CB, and n-PH had 20, 17, and 11 times greater vascular volume fraction than adult, respectively. Moreover, thickness of blood vessels, in three regions, was six times higher in adults than in neonatal. a-PH appeared to have higher vascular fraction, longer and thicker blood vessels than both a-AH and a-CB. Overall, neonatal regions had a higher number of blood vessels, more branching, and higher tortuosity compared to adult regions. For the first time, critical point drying-based μ CT imaging allowed detailed three-dimensional visualization and quantitative analysis of vascularized meniscal structures. We showed more vascularity in neonatal menisci, while adult menisci had fewer and thicker vascularity especially limited to the femoral surface.

KEYWORDS

contrast agent-free microcomputed tomography, meniscus microstructure, osteoarthritis, vascularization

1 | INTRODUCTION

The menisci are C-shaped fibrocartilaginous tissues located in the knee joint. They are known to have a primary function in biomechanical properties of the knee joint, like load bearing, joint stability, and shock absorption.¹⁻³ These properties are provided by a complex collagenous extracellular matrix (ECM) organization, that include water-binding proteoglycans and vascular supply.¹⁻³ However, menisci are prone for degeneration, usually caused by tearing from trauma or osteoarthritis (OA). After any kind of degeneration has happened, the spontaneous healing possibilities of meniscus are weak due to the limited vascular supply.^{4,5}

In a developed meniscus “red-red,” “red-white,” and “white-white”—zones can be identified based on their assessment of blood supply with each zone radially covering approximately a third in developed meniscus.⁶⁻⁸ The peripheral red-red zone is composed of a high vascular supply; the red-white zone in the middle third has limited vascular supply, and finally, the inner third, the white-white zone, is completely avascular. The highly vascularized red-red zone retains the ability to spontaneously heal damage, while in the inner avascular area, the healing potential remains low with and without pre-emptive surgery. Overall, vascular supply through the meniscal tissue is suggested to have an important role in the healing of the meniscus through revascularization and overall increased healing in the outer red-red regions of the meniscus.^{5,9-12}

Previous studies have reported that vascularity decreases with increasing age in human menisci.^{7,13-16} The high degree of vascularity is important for the early growth and maturation of the meniscus, with blood supply covering most of the meniscus width and length.¹⁷ However, in the developed meniscus of adults, only the outer third remains vascularized to some extent in both animals and humans.¹⁸ In addition, regional differences have been found between the horns and body of the menisci with more vascularization found near the horns of the meniscus, that reside further away from the load-bearing areas.^{1,7,19}

We have previously shown that human meniscal microstructures can be visualized and quantitatively analyzed with microcomputed tomography (μ CT) using drying-based sample processing.^{20,21} Here we utilized critical point drying (CPD) as an alternative method for hexamethyldisilazane (HMDS) to remove water from the tissue and preserve the structural integrity of meniscus. This allows visualization of meniscus and its' vascular structures with x-ray imaging without chemical contrast-enhancing agents. However, the vascular supply of the porcine meniscus has not been quantitatively analyzed three-dimensionally (3D).

In this study, our objectives were to quantitatively analyze the vascular supply of ex vivo porcine meniscus samples in 3D using CPD-based μ CT imaging protocol between neonatal and adult tissues and their respective regions: anterior horn, central body, and posterior horn. In addition, we performed immunohistochemical staining with the antibody against CD31 to visualize the meniscal vascularization in cut two-dimensional (2D) sections and compared the stained sections with μ CT cross-sectional images to validate the vascular segmentations. We

focused on the medial meniscus as it is more vulnerable to meniscal tearing and degeneration when compared to the lateral meniscus.²²

2 | METHOD

2.1 | Tissue sample preparation

Medial porcine meniscus specimens from 10 neonates were collected from stillbirth male and female pigs provided by a local breeding farm. We also selected 10 medial porcine meniscus specimens from adult (3–4 years old) female pigs from a local slaughterhouse. The neonatal menisci specimens were chosen to represent a group of completely vascularized menisci, or not fully developed neonatal population, while the 3- to 4-year-old menisci specimens are fully developed and thus were chosen to represent the adult population. The samples were cleaned under a sterile hood in phosphate-buffered saline (PBS; Thermo Fisher Scientific) and fixed for at least 14 days in 10% neutral buffered formalin (Bio-Optica Milano). All menisci were radially sectioned into three anatomical regions: anterior horn, central body, and posterior horn. A diagram of how the regions were sectioned is shown in Supporting Information S1: Figure 1. Hereafter, these neonatal and adult anatomical regions are referred to as n-AH (neonatal anterior horn), n-CB (neonatal central body), n-PH (neonatal posterior horn), and a-AH (adult anterior horn), a-CB (adult central body), and a-PH (adult posterior horn), respectively. The adult specimens were further cut into two 4-mm-thick tissue sections (measured from the outer side), for μ CT imaging and histological sample processing. The neonate specimens were cut similarly but on a smaller scale. No animals were killed for the purposes of this study: all cadavers were used according to the principles stated by the EC Directive 86/609/EE about the protection of animals used for experimental and other scientific purposes.

2.2 | Immunohistochemical validation of vascularity

Fixed histology specimens were washed for half an hour in running water and decalcified for at least 5 days in a solution consisting of citric (7.5% Sigma-Aldrich) and formic acid (25%, DITTA). The samples were washed again in running water for one and a half hours, in distilled water for 30 min, and dehydrated in an increasing scale of ethanol (70% overnight [O.N.], 80% 30 min, 95% 60 min, 2 \times 100% 45 min). They were then clarified in xylene (two 45-min washes) and embedded in paraffin for sectioning. The sections were cut and stained with vascular-related markers in immunostaining. The anti-CD31 antibody (Abcam) was used as a vascular marker as described by Canciani et al.²³ Briefly, sections were deparaffinized in xylene followed by a descending scale of alcohols to water (2 \times xylene 5 min, 2 \times 100% ethanol 5 min, 95% ethanol 5 min, 70% ethanol 5 min, distilled water 5 min). Endogenous peroxidase blocking was performed with 10% hydrogen peroxide (H_2O_2) for 10 min and a

5-min PBS wash was performed. A pH 6 citrate buffer retrieval for 5 min in the microwave followed by half an hour of cooling was performed twice. One hour of blocking with 10% Normal Goat Serum (NGS; Thermo Fisher Scientific) preceded incubation with the antibody diluted 1:50 in PBS + 10% NGS O.N. at +4°C overnight. The following day the slides were washed in PBS for 5 min and incubated with Envision anti-rabbit (Dako EnVision+ System-HRP, K4002) for 3 h at room temperature (RT). To develop, 3,3'-diaminobenzidine (DAB; Thermo Fisher Scientific) was used (18 min). The samples were then counterstained with Meyer's hematoxylin for 2 min and rehydrated in an increasing scale of alcohols and clarified in xylene. Finally, Eukitt mounting medium (Sigma-Aldrich) was used to mount the coverslip. B-1000 Optika microscope (OPTIKA) was employed to acquire the images. The described immunohistochemical method was used as a validation for the μ CT method.

2.3 | μ CT imaging of meniscal vascularization

After fixation, the μ CT pieces were dehydrated in an ascending ethanol series (30%–50%–70%–80%–90%–96%–100%) for a minimum of 4 h in each step. To obtain optimal soft tissue contrast for μ CT imaging, samples were dried using a critical point drying (CPD) device (K850; Quorum). Image acquisition was conducted with a desktop μ CT system (SkyScan 1272; Bruker microCT) with the following settings: tube voltage 40 kV; tube current 250 μ A; no additional filtering; isotropic voxel size 3.3 μ m; the number of projections 2384; averaging three frames/projection; and exposure time 1515 ms. Image reconstruction was done with NRecon software (v1.7.1.6. Bruker microCT) with beam-hardening and ring-artifact corrections applied.

2.4 | Volumetric 3D analysis of meniscal vascularization

For each sample, cross-sectional μ CT images were used for the 3D segmentation of vascularity in the meniscus using Dragonfly (Version 2022.1; Object Research Systems (ORS) Inc). Although the vascularity was not stained with a specific contrast agent, the CPD-based drying process gave it a distinct contrast difference when compared to the surrounding collagenous extracellular matrix. Moreover, distinct morphology and connected network of blood vessels allowed segmentation of the vascularity. Thus, local thresholding together with manual segmentation was used to attain the vascularized volumes. Furthermore, despeckling was used to remove noise. We produced vascular volumes of all samples and measured four descriptive parameters for vascularity: (a) vascular volume fraction, that is, the ratio of segmented vascularity to the total volume of meniscus, (b) average blood vessel thickness, (c) blood vessel penetration depth, and (d) total tissue volume that was calculated to clarify the size relationship between the groups. The penetration

depth of blood vessels was calculated as a fraction of the maximum radial depth of the meniscus width. A schematic of how volumes and fractions are calculated from 3D volumes and cross-sectional images is seen in Supporting Information S1: Figure 2. 3D volumetric analysis of the segmented vascularity was performed using CTAn (version 1.20.3; Bruker MicroCT). Visualization of 3D μ CT-images was done with CTVox (version 3.3.0; Bruker MicroCT).

2.5 | Quantitative 3D analysis of vascular network

To quantify the vascular branching in the samples, the segmented vascularity was skeletonized, analyzed, and visualized with Dragonfly software (ORS). A total number of blood vessel segments, their number of branching points, average segment lengths, and tortuosity were measured to describe the vascular network in 3D. Tortuosity is calculated for each blood vessel segment as the distance between the segment endpoints divided by Euclidean distance (shortest path).

2.6 | Identification of meniscal calcifications

Few adult menisci were found inhabiting calcified structures in the μ CT images. We refined our previously used calcification analysis method where we had identified calcifications from meniscus together with μ CT and histology.²⁴ In this study, we identified similar particles and identified them as calcifications based on their high density compared to surrounding soft tissue, their location inside the meniscus, and their crystal-shaped morphology and size.

2.7 | Statistical analyses

Statistical analysis was performed using GraphPad Prism 8 (GraphPad Software, Inc.). Group-wise comparison of estimated means between anatomical regions of the meniscus was conducted with a Linear Mixed Model in Prism Graphpad (V. 8.4.2) with matching anatomical regions within single meniscus (n-AH vs. n-CB vs n-PH), assumption of sphericity, and with Bonferroni correction. Group-wise comparison of estimated means between age groups of menisci (n-AH vs. a-AH) was done with Geisser-Greenhouse sphericity correction and Bonferroni correction. The descriptive data of menisci are provided in scatterplots with 95% confidence intervals (95% CIs). Estimated means and estimated differences between groups are provided in Supporting Information S1: Tables I–IV.

3 | RESULTS

3.1 | μ CT imaging of meniscal vascularization

Representative 2D immunohistology images, 2D μ CT slices of adjacent meniscus pieces, and 3D visualization of μ CT images are

displayed in Figure 1. Visual evaluation of both μ CT cross-sectional images and CD31 immunohistology showed similar morphology and size in blood vessels between methods (Figure 1A vs. B, D vs. E, G vs. H, J vs. K, white arrows). The CPD-based drying method seems to preserve the tissue and vascular network intact for accurate μ CT imaging. Branching and more complex vascularity networks can only be seen in 3D from μ CT visualization compared to standard histology (Figure 1C,F,I,L).

The vascularization network in CPD-treated meniscal samples was successfully depicted in 3D using μ CT imaging. In Figure 2, we show example images of μ CT 3D volumes from neonatal and adult porcine menisci, their regions, and their segmented vascularization. Specifically, Figure 2A shows the 3D scan of the tissue, Figure 2B shows the vessels inside the meniscus, and Figure 2C shows the isolated vascular network, clearly highlighting the differences between the neonatal and the adult. The vascular network in the neonatal spreads from the outer to the inner region, while in the adult it is limited to a few vessels in the outer region, mostly located on the femoral side (Supporting Information S1: Videos S1 and S2; Figure 2E, black arrow).

3.2 | Immunohistochemistry—validation of vascularity

The presented results of the CD31-stained immunohistology slices were used to validate the μ CT segmentations. CD31 immunostaining

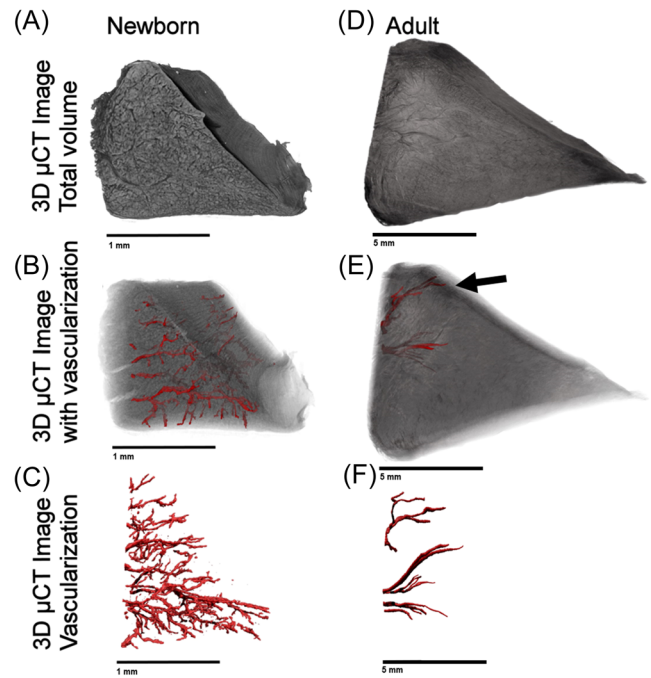


FIGURE 2 Representative μ CT 3D volumes from the posterior horn of neonatal (A)–(C) and adult groups (D)–(F). Meniscal vascularization displayed together with soft tissue shows higher vascularity in the neonatal group (B), penetrating throughout the whole meniscus, while the adult group is found only in the outer third, mostly on the femoral side (E, black arrow). The analyzed meniscal vascularization was depicted in neonates (C) and adults (F). 3D, three-dimensional; μ CT, microcomputed tomography.

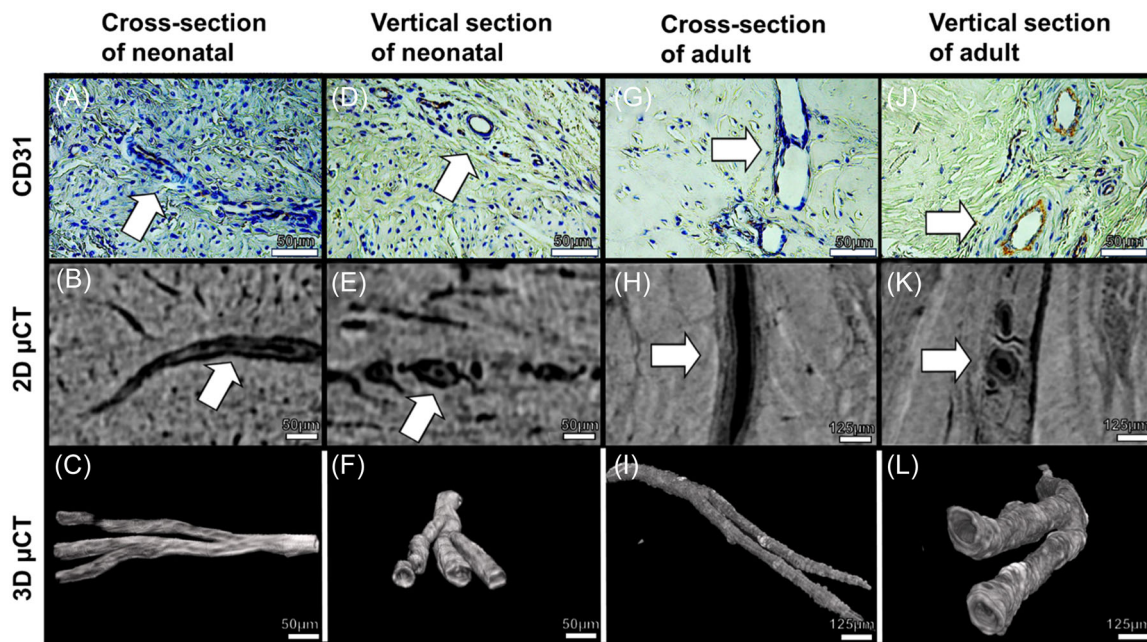


FIGURE 1 The representative posterior horn of 2D immunohistology image (A), (D), (G), and (J), 2D μ CT slices of adjacent meniscus piece (B), (E), (H), and (K), and 3D visualization of μ CT images (C), (F), (I), and (L) of both neonatal (A)–(F) and adult (G)–(L) in vertical (A)–(C), (G)–(I) and cross-sectional (D)–(F), (J)–(L) slices. Assessment of blood vessels shows similar morphology and size between μ CT-images and CD31-stained histological slices. In addition, the walls and lumen of blood vessels are well visible. Thicker and larger blood vessels of adult menisci can be seen in both histological and μ CT-images. 2D, two-dimensional; μ CT, microcomputed tomography.

allowed the identification of blood vessels in the tissue. In the neonatal menisci, blood vessels were identified throughout the tissue, both in the inner zone (Figure 3A, black circles with blood vessels) and the outer zone (Figure 3B, black circles with blood vessels); while in the adult menisci, the inner zone appears completely devoid of blood vessels (Figure 3C) which, however, remain in the outer zone (Figure 3D, black circles with blood vessels). This was similar in all three meniscal regions (PH, CB, and AH).

3.3 | Volumetric 3D analysis of meniscal vascularization

In quantitative measurements of the vascular volume fraction, the anterior horn, central body, and posterior horn of the neonate were greater than the adult, respectively (AH: $p < 0.001$, CB: $p < 0.001$ and PH: $p < 0.001$) (Figure 4A). In neonatal group, n-AH had a higher vascular fraction compared to n-PH ($p < 0.05$, Figure 4A), but no differences were observed between n-CB and n-AH. a-PH had higher vascular fraction when compared to both a-AH and a-CB. ($p < 0.01$, Figure 4A).

In the thickness measurements of blood vessels, in the three regions (AH, CB, and PH) the adult had an average thickness of about six times higher than the neonatal ($p < 0.001$, Figure 4B). In Figure 4B, we found that the average blood vessel thickness in adult menisci was highest in a-PH group when compared to a-AH and a-CB, respectively ($p < 0.001$, Figure 4B).

The depth of penetration of the vessels into the tissue was drastically reduced in the transition from the neonatal to the adult animal in the three regions ($p < 0.001$, Figure 4C), but no differences between them neither in the neonatal nor in the adult (Figures 4C).

Total tissue volume of meniscus was measured to clarify the size differences between the groups and regions. All three adult regions (AH, CB, and PH) had higher total tissue volume when compared to their respective neonatal regions ($p < 0.001$, Figure 4D). In neonatal group, n-AH had higher tissue volume when compared to n-CB ($p < 0.01$). Estimated differences between groups of each parameter are found in Supporting Information S1: Tables I and II.

3.4 | Quantitative 3D analysis of vascularization network

Representative visualization of skeletonized 3D vascular network are displayed in Figure 5. Quantitative measurements of blood vessel segments showed the number of segments was greater in all neonate groups (AH, CB, and PH: $p < 0.001$) when compared to corresponding adult groups (Figure 6A). Within the same age group, n-AH and n-PH regions had greater number of segments when compared to n-CB (n-AH vs. n-CB $p < 0.001$ and n-PH vs. n-CB $p < 0.05$, respectively). In the adult group, a-PH had greater number of segments when compared to a-CB ($p < 0.05$).

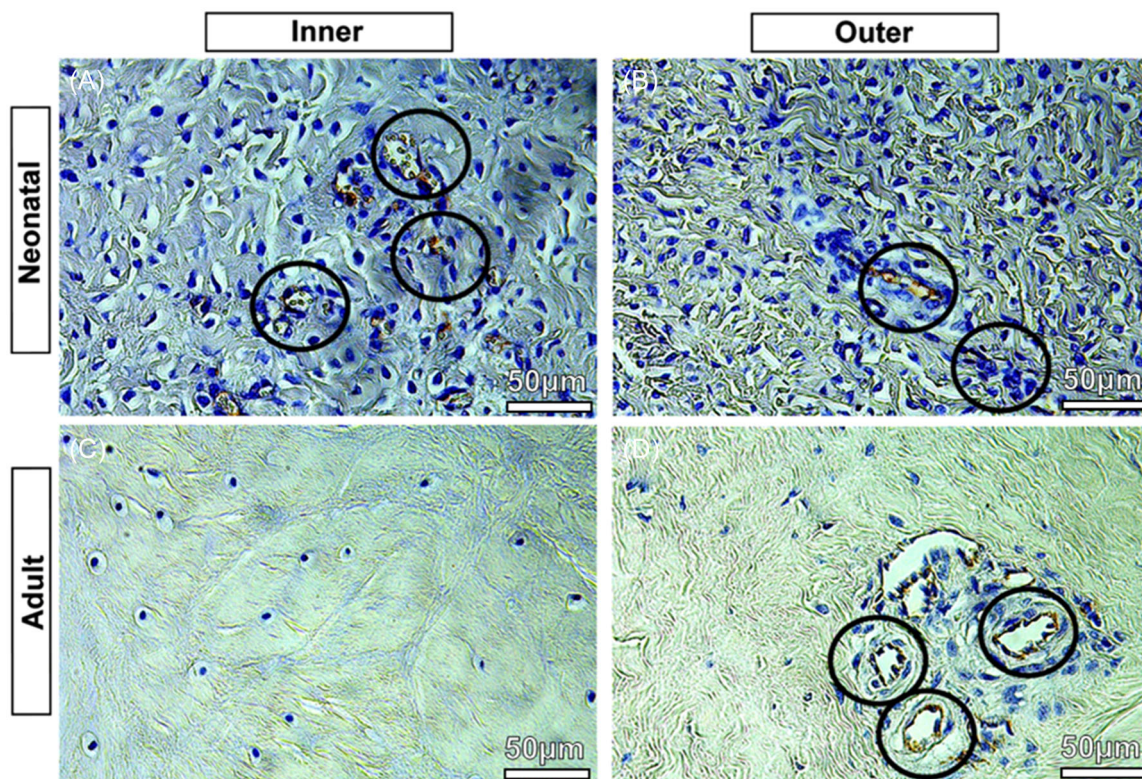


FIGURE 3 CD31 immunohistochemical staining of neonatal (A) and (B) and adult (C) and (D) porcine meniscus; representative images of the posterior horn. Black circles indicate blood vessels containing red blood cells. Scale bar: 50 μ m.

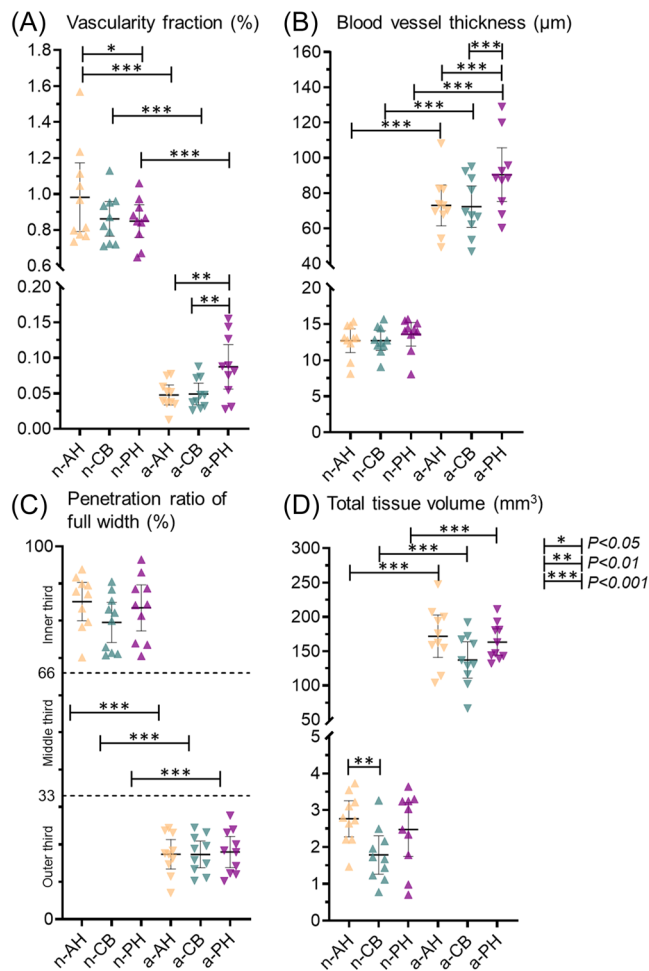


FIGURE 4 (A) Vascular fraction comparison of tissue fraction. (B) Blood vessel thickness. (C) Penetration depth of blood vessels in ratio of radial tissue length. (D) Total tissue volume of the meniscus to clarify the size relationship between the groups. Comparisons were done between neonatal and adult meniscus in their anatomical region (AH, anterior horn; CB, central body; PH, posterior horn). Group-wise comparison of estimated means between anatomical regions of the meniscus was conducted with a Linear Mixed Model in Prism Graphpad (V. 8.4.2) with matching anatomical regions within a single meniscus (n-AH vs. n-CB vs. n-PH). Group-wise comparison of estimated means was done between age groups of menisci (e.g., n-AH vs. a-AH). $N = 10$, data are expressed as mean \pm 95% confidence interval. *** $p < 0.001$.

The number of branches was greater in all neonate groups (AH, CB, and PH: $p < 0.001$) when compared to the corresponding adult group (Figure 6B). In the neonate group, anterior and posterior regions had more branches when compared to the central region ($p < 0.01$). No differences were found between the adult groups.

The average blood vessel segment length was greater in all adult groups (AH, CB, and PH: $p < 0.001$) when compared to the corresponding neonate group (Figure 6C). In the neonate group, the anterior horn had the longest blood vessel segments on average when compared to both central and posterior groups ($p < 0.05$). In the adult group, the posterior horn was greater when compared to both anterior and central groups ($p < 0.05$).

Tortuosity was greater in all neonate groups (AH, CB, and PH: 0.001) when compared to corresponding adult groups (Figure 6D). No differences were observed between regions in their respective age groups. Estimated differences between groups are found in Supporting Information S1: Tables III and IV.

3.5 | Calcifications

Incidentally, we found calcified clusters in three samples of the a-AH group. In Figure 7, we present the scatterplot of vascular fraction between calcified and non-calcified tissue. After splitting the a-AH group, we see that the calcified group ($n = 3$) had a seemingly higher vascular fraction when compared to non-calcified anterior horns ($n = 7$). However, we did not perform any statistical analysis for these as the number of samples in the calcified group was low.

4 | DISCUSSION

CPD-based sample drying protocol together with high-resolution μ CT imaging is a feasible method to visualize and quantitatively analyze the vascular network of porcine meniscus in 3D. The results of volumetric analyses indicate not only substantial differences in vascular supply between neonatal and adult groups, but also regional differences between anterior horn, central body, and posterior horn. Decreased vascular content in adult groups confirms a strong association between age and vascularity of meniscus already observed in our previous research in pigs' developmental studies.^{25–27} Furthermore, vascularity seems to decrease the most in the anterior horn and least in the posterior horn of the meniscus with age, suggesting regional differences. To our knowledge, this is the first study to quantitatively study the vascularization in 3D between neonatal and adult porcine menisci considering the three zones.

From our volumetric μ CT analyses, we found a higher vascularity volume fraction in the neonatal menisci when compared to adult menisci, suggesting a decrease in vascular volume fraction with age. Our findings are supported by previous cadaver studies measuring vascular density, where overall vascular density decreased with increasing age in human menisci.^{14,15,28,29} In our study, the neonatal menisci were seemingly less wedge-shaped and relatively thicker radially compared to the developed wedge-shaped adult menisci. The neonatal meniscus has been reported to have more heightened surfaces compared to the wedge-shaped developed adult meniscus.²⁸ Similarly, the tortuosity in the neonatal groups was higher compared to adult vessels, suggesting more curved and complex blood vessels are inhabiting inside the neonatal menisci, compared to the straighter shape found in the adult menisci. Furthermore, in our previous study, we reported that age-related angiogenesis factors are highly expressed in neonatal porcine meniscus.²⁵ The reason for a sharp decrease in vascularity after birth has been thought to be derived from the start of biomechanical stress and loading in the meniscus after birth, especially in the inner white zones causing extrusion in the meniscus.²⁸ Nutrition

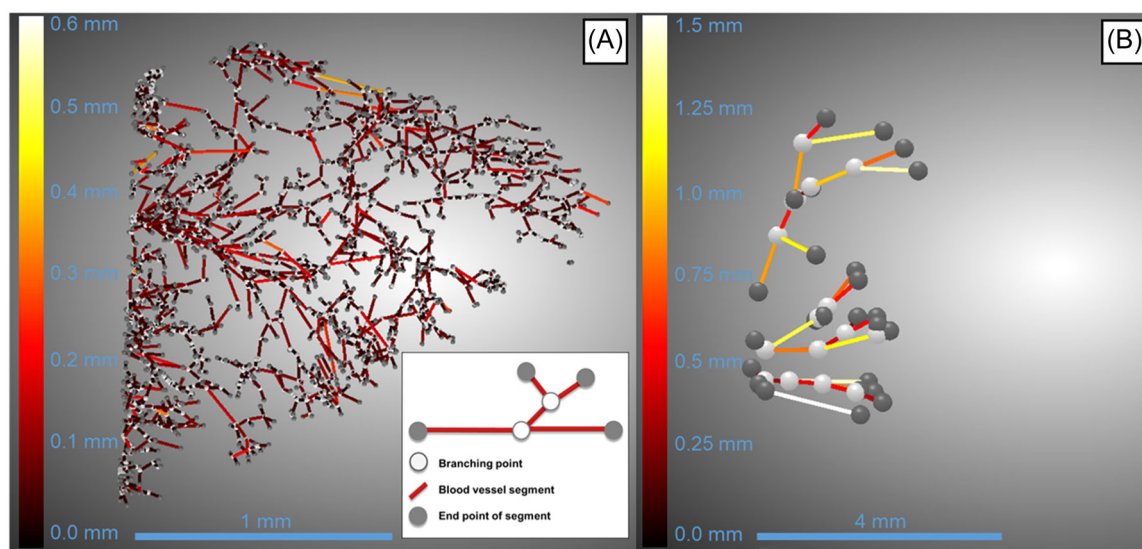


FIGURE 5 Representative images of skeletonized vascular networks of neonatal (A) and adult (B). White spheres show branching points where blood vessels split into two or more segments, while gray spheres indicate the end point of vessels. Blood vessel segment length is shown on the left scale. Neonatal vascular network consists of a high number of interconnected branches and segments when compared to adult vascular network.

via diffusion through a large vascularization network in the meniscus is important before the loading starts around 2 years of age in humans, after which the nutrition of these areas occurs via diffusion.²⁸ If meniscus tears or degenerates, nutrition is required for healing, possibly leading to revascularization in the form of increased vascular volume and blood flow as a response to injury.³⁰ In OA, it has been identified to promote angiogenesis and increase vascularity in the knee joint and meniscus.^{31–33} Moreover, meniscal lesions have also been reported to cause inflammation and swelling in the OA tissue.³⁴ Thus, the revascularization to heal tears in avascular areas in healthier and compressed tissue may be suppressed by tightly organized collagenous ECM, while revascularization could manifest more easily in more degenerated, sparser tissue where reparative cells can infiltrate the tissue.³⁵ Similarly, revascularization is essential in successful meniscal allograft transplantations. Studying the effect of revascularization in allografts with μ CT could be a beneficial 3D method in the future.

In the neonatal group, the anterior horn had the highest vascular fraction, while in the adult group, the posterior horn had retained the highest vascular fraction. Our vascular network analyses showed that the neonatal vascular network consists of a higher number of interconnected blood vessel segments and branches when compared to the adult vascular network. In addition, both anterior and posterior horn of neonatal meniscus had higher number of blood vessels and branching when compared to central body. Higher vascularity near the horns of the meniscus could be expected as major arteries reside closer to the horns in the periphery capsule of meniscus, supplying the blood vessels.^{1,7,8,36,37} Anatomically, the limited blood supply originates mainly from the medial and lateral geniculate arteries: the radial branches, which enter the meniscus at intervals, mainly supply the anterior horn and the posterior horn.^{38,39} However, in our study, the largest decrease in vascular content was found in the anterior

horn between neonatal and adult groups, while the posterior horn retained the most vascularity. The posterior horn of adults inhabiting most vascular content is supported by our previous study showing that posterior horn of adult meniscus regions corresponded to the highest vascular cell activity.⁴⁰ It has been studied that in the medial meniscus of humans, the anterior horn is subjected to higher stresses in gait and shows greater stiffness compared to the posterior horn.^{41–43} This could suggest that lower stress and compressive forces in the porcine gait cycle are localized to the posterior horn, leaving space for thicker and longer vascular organization. Quantifying how vascularity decreases in the meniscus as the knee is exposed to biomechanical loading could be interesting to study in the future.

We found that blood vessels radially penetrated through most neonatal menisci while in adult menisci they covered less than a third of meniscal tissue, reaching only the outer red-red zone. These results are supported by our previous angiogenic expression study, where we reported that vascular endothelial growth factor (VEGF), which is a specific mitogen for vascular endothelial cells, is evenly expressed between inner, middle, and outer neonatal porcine menisci regions, but significantly increased from inner to the outer part of adult menisci.²⁵ Similar results between VEGF expression, our CD31 vascular stain, and our vascularity penetration depth analysis suggest that using μ CT imaging can produce important 3D information for the development of degenerative changes or the healing of meniscal transplants.^{44,45} Our results regarding the penetration depth of blood vessels in the adult specimens correlate with that of adult humans, with vessels entering and penetrating only the outer meniscal third or quarter.²⁸ In our study, the neonatal menisci show a similar pattern of vascularity as in the meniscus of a neonatal human in a previous study.²⁸ In addition, biomechanical studies have reported similarities in porcine and human meniscus tensile and compression properties and permeability.^{43,46–48}

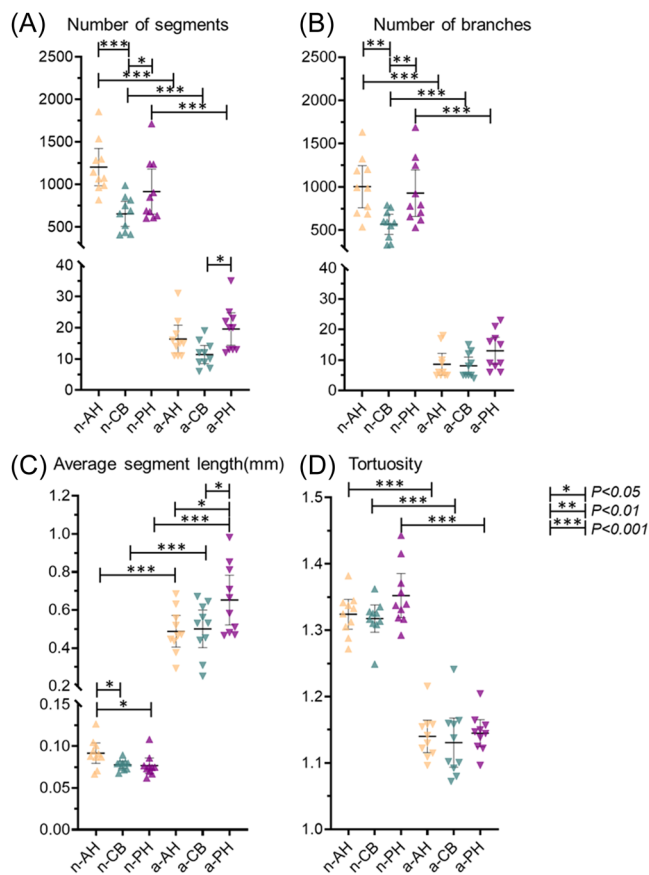


FIGURE 6 (A) Number of blood vessel segments. (B) Number of branching points. (C) Average segment length (mm). (D) Tortuosity of blood vessel segments. Comparisons were done between neonatal and adult meniscus in their anatomical regions (AH, anterior horn; CB, central body; PH, posterior horn). Group-wise comparison of estimated means between anatomical regions of the meniscus was conducted with a Linear Mixed Model in Prism Graphpad (V. 8.4.2) with matching anatomical regions within a single meniscus (n-AH vs. n-CB vs. n-PH). Group-wise comparison of estimated means was done between age groups of menisci (e.g., n-AH vs. a-AH). $N = 10$, data are expressed as mean \pm 95% confidence interval. *** $p < 0.001$.

Therefore, the porcine meniscus shared similar biomechanical and vascular properties to the human meniscus and could be used as a suitable model for fast translation from the pig to the human.^{43,46,47}

Interestingly, in the adult posterior horn, the blood vessels were found to be thicker and longer when compared to anterior horn and central body. In adult porcine, we observed the vascular network is limited to a few vessels in the outer region, mostly located on the femoral side. Blood vessels from large arteries enter the meniscus along the tie-fibers.⁴⁹ We observed similarly that blood vessels penetrate the meniscal tissue along or inside the radial tie-fibers. Arnoczky et al observed that a vascular network extends for a short distance on both the femoral and tibial surfaces of the menisci but does not contribute to nourishing the meniscal stroma.⁶ The same authors found similar vascularization patterns in the two horns. In a previous study of our group, we found that the femoral surface of adult pig meniscus is characterized by a higher quantity of GAGs with

the interposition of radial and oblique fibers.⁵⁰ These features are responsible for higher resistance to compressive forces like those acted on by the femoral condyles. However, the tibial surface shows a circumferential arrangement of the fibers and a poorer GAG presence and cellular spread. The greater vascularization observed on the femoral side compared to the tibial side is necessary to support the nutritional needs of a greater number of cells on the femoral side, as well as being compliant with the different mechanical functions of the two sides of the meniscus. Moreover, these characteristics seem to allow a higher resistance of the tibial surface to tensile forces.⁵⁰ Therefore, these results together suggest that a higher vascularization is associated with a greater number of cells that can produce a greater quantity of GAGs and respond to the compressive forces that act upon the femoral condyles. Moreover, a lower vascularization is associated with a lower number of cells, in an area where the production of circumferential fibers is prevalent compared to the production of GAGs to unload and redistribute the compressive forces to the underlying bone.

CPD-based μ CT imaging protocol was validated using CD31-stained immunohistology. CPD treatment seemingly preserved the tissue when compared to the immunohistology with blood vessels being visible in both immunohistology and μ CT images while sharing similar morphology and size. Qualitatively, both immunostaining and μ CT showed fully vascularized neonatal menisci while vascularity in adult menisci seemed to only contain vessels in the outer region. Branching and more complex vascularity networks can be seen in 3D from μ CT visualization. Importantly, branching and 3D structures can only be detected using μ CT-imaging compared to the standard 2D immunohistology. However, immunohistology is an important complementary method when using μ CT in identifying tissue structures, that do not necessarily have different attenuating properties in μ CT images.

As an incidental finding, we found clusters of calcifications in three anterior horns of adult pigs, two of which were in the red-red zone near the blood vessels and one in the inner white-white region of the meniscus. In early OA, increased expression of VEGF and angiogenesis promotes vascular content leading to ossification in the articular cartilage.^{33,51} Moreover, we have seen similar calcifications in our previous study where we showed the feasibility of quantitative studies of the calcified meniscus in 3D with μ CT and found that calcification volume in the meniscus increases with increasing histopathological degeneration.²⁴ Our findings show that all three samples inhabiting calcifications also had the highest ratio of the vascular fraction of the anterior horn in adults, suggesting correlation a between meniscus angiogenesis and ossification in the medial anterior horn. While it is possible to do quantitative analysis of the meniscal calcifications using μ CT imaging, characterizing the crystal type requires another modality, for example, Raman spectroscopy or x-ray diffraction.^{52,53} Thus, the presented method of μ CT imaging enables imaging of denser tissues like calcification together with soft tissues and their vascular structures and could be used to study the effects of ossification and angiogenesis in the meniscus in the future.

Adult animals used in our studies are heavy pigs (<250 kg), as they are produced for food production. High body mass index (BMI)

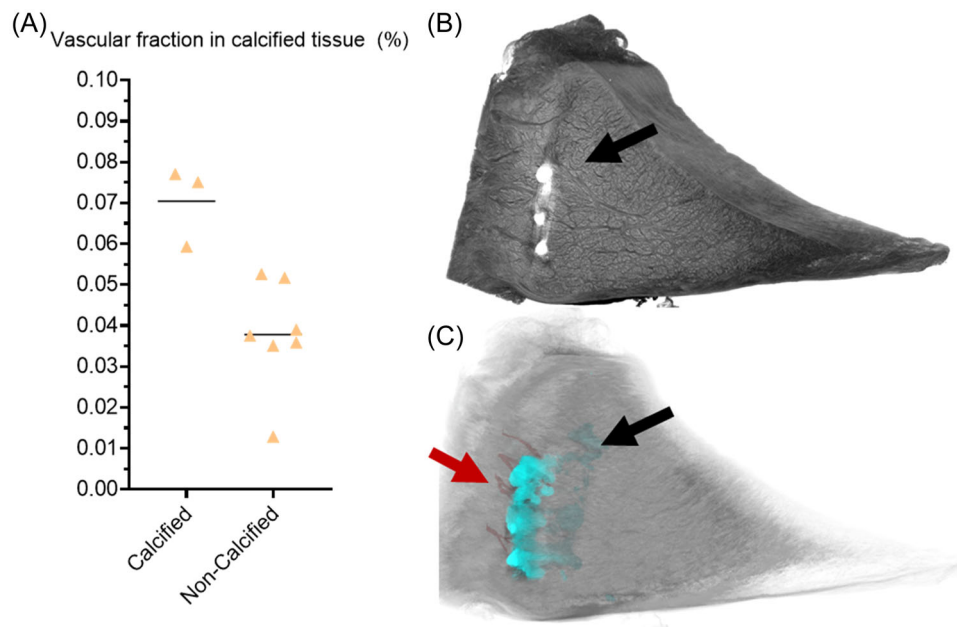


FIGURE 7 (A) Mean vascular fraction (%) in the anterior horn of adult porcine meniscus (a-AH) between calcified and noncalcified tissue. Calcified menisci had a higher average vascular fraction denoting higher vascularity overall compared to noncalcified menisci. (B) 3D μ CT image of the medial anterior horn of adult pig meniscus with calcification clusters inside the tissue in the outer region (black arrow). (C) 3D μ CT image showing calcified structures colored in blue (black arrow) inside the meniscus together with vascularization (red arrow). 3D, three-dimensional; μ CT, microcomputed tomography.

and age have been studied to have a significant role in the risk of meniscus injury and OA in both humans and animals.^{54–58} Furthermore, our findings of possible revascularization together with ossification in the anterior horn of the medial meniscus of adult pigs suggest a manifestation of early-stage OA. Thus, following the 3Rs, developing a combined early OA and obesity research model based on overweight pigs used in food production could prove a beneficial and sustainable research model option for future studies.

The present study has some important limitations. First, the CPD-based sample drying method preserves the tissue morphology and enables μ CT imaging but does cause some shrinking and may not perfectly reflect the sample *in vivo*.⁵⁹ Secondly, the incidental calcifications in the menisci can cause streaking artifacts to the image due to differences in soft and hard tissue attenuation, decreasing image quality. Furthermore, the calcified menisci have seemingly higher vascular content compared to non-calcified tissue in the same group, affecting the a-AH group average in vascular volume and fraction measurements. However, in OA, angiogenesis has been suggested to promote endochondral ossification in porcine cartilage, thus spontaneous calcifications in the porcine meniscus could be expected.⁶⁰ Third, we did not separate the neonatal porcine between male and female when extracting their menisci. Lastly, our CPD-based μ CT imaging can only be performed on extracted tissues and cannot therefore be used to monitor changes in vascularity over time.

In conclusion, μ CT imaging allows detailed quantitative volumetric analysis of vascularized meniscal structures in porcine neonatal and adult menisci. In the future, this method could be used to understand the meniscus regeneration and degeneration concerning

vascular anatomy in the context of vascular diseases, hypertension, healing of meniscal transplants, and arthritis, or simply for the clinical study of the aged meniscus, which is often accompanied by increased vascularization. In conclusion, μ CT imaging allows detailed quantitative volumetric analysis of vascularized meniscal structures.

AUTHOR CONTRIBUTIONS

Conception and design: Ville-Pauli Karjalainen, Valentina R. Herrera Millar, Ali Mobasheri, Alessia Di Giancamillo, Mikko A. J. Finnilä. *Provision of study materials and tissue preparation:* Ville-Pauli Karjalainen, Valentina R. Herrera Millar, Margherita Pallaoro. *Micro-CT imaging:* Ville-Pauli Karjalainen, Valentina R. Herrera Millar, Khaled Elkhoully. *Image processing/assessment:* Ville-Pauli Karjalainen, Khaled Elkhoully. *Statistical analysis:* Ville-Pauli Karjalainen, Valentina R. Herrera Millar. *Interpretation of results:* All coauthors. *Drafting of the article:* Ville-Pauli Karjalainen, Valentina R. Herrera Millar. *Critical revision of the article for important intellectual content:* All coauthors. *Final approval of the article:* All coauthors.

ACKNOWLEDGMENTS

V.-P. K. has received a grant from Finnish Cultural Foundation (SKR). M. A. F. would like to acknowledge funding from Jane and Aatos Erkko Foundation and Academy of Finland (347445 and 353755). The authors further acknowledge the help of Dragonfly—software (Object Research Systems [ORS] Inc.) in the use of image segmentations.

CONFLICT OF INTEREST STATEMENT

The authors declare no conflict of interest.

ORCID

Ville-Pauli Karjalainen  <https://orcid.org/0000-0001-8376-2454>

Khaled Elkhouly  <https://orcid.org/0000-0001-8345-4742>

Simo Saarakkala  <https://orcid.org/0000-0003-2850-5484>

Ali Mobasheri  <https://orcid.org/0000-0001-6261-1286>

Alessia Di Giancamillo  <https://orcid.org/0000-0003-1674-3020>

Mikko A. J. Finnilä  <https://orcid.org/0000-0002-3348-5759>

REFERENCES

1. Fox AJS, Bedi A, Rodeo SA. The basic science of human knee menisci: structure, composition, and function. *Sports Health*. 2012;4(4):340-351.
2. Kelly MA, Fithian DC, Chern KY, Mow VC. Structure and function of the meniscus: basic and clinical implications. In: Ratcliffe A, Woo SLY, Mow VC, eds. *Biomechanics of Diarthrodial Joints*. Springer; 1990:191-211.
3. Messner K, Gao J. The menisci of the knee joint. Anatomical and functional characteristics, and a rationale for clinical treatment. *J Anat*. 1998;193(2):161-178.
4. Arnoczky SP, Warren RF. The microvasculature of the meniscus and its response to injury: an experimental study in the dog. *Am J Sports Med*. 1983;11(3):131-141.
5. Hennerbichler A, Moutos FT, Hennerbichler D, Weinberg JB, Guilak F. Repair response of the inner and outer regions of the porcine meniscus in vitro. *Am J Sports Med*. 2007;35(5):754-762.
6. Arnoczky SP, Warren RF. Microvasculature of the human meniscus. *Am J Sports Med*. 1982;10(2):90-95.
7. Day B, Mackenzie WG, Shim SS, Leung G. The vascular and nerve supply of the human meniscus. *Arthroscopy*. 1985;1(1):58-62.
8. Danzig L, Resnick D, Gonsalves M, Akeson WH. Blood supply to the normal and abnormal menisci of the human knee. *Clin Orthop Relat Res*. 1983;172:271-276.
9. Howell R. Degenerative meniscus: pathogenesis, diagnosis, and treatment options. *World J Orthop*. 2014;5(5):597.
10. Peretti GM, Gill TJ, Xu JW, Randolph MA, Morse KR, Zaleske DJ. Cell-based therapy for meniscal repair. *Am J Sports Med*. 2017;32(1):146-158. doi:10.1177/0095399703258790
11. Kobayashi K, Fujimoto E, Deie M, Sumen Y, Ikuta Y, Ochi M. Regional differences in the healing potential of the meniscus—an organ culture model to eliminate the influence of microvasculature and the synovium. *Knee*. 2004;11(4):271-278.
12. Jakob RP, Stäubli HU, Zuber K, Esser M. The arthroscopic meniscal repair. Techniques and clinical experience. *Am J Sports Med*. 1988;16(2):137-142. doi:10.1177/036354658801600208
13. Petersen W, Tillmann B. Collagenous fibril texture of the human knee joint menisci. *Anat Embryol*. 1998;197(4):317-324.
14. Clark CR, Ogden JA. Development of the menisci of the human knee joint. Morphological changes and their potential role in childhood meniscal injury. *J Bone Joint Surg*. 1983;65(4):538-547.
15. Michel PA, Domnick CJ, Raschke MJ, et al. Age-Related changes in the microvascular density of the human meniscus. *Am J Sports Med*. 2021;49(13):3544-3550.
16. Lin KM, Gadinsky NE, Klinger CE, et al. Increased vascularity in the neonatal versus adult meniscus: evaluation with magnetic resonance imaging. *Cartilage*. 2021;13(2_suppl):1562S-1569S.
17. Sanchez-Adams J, Athanasiou KA. The knee meniscus: a complex tissue of diverse cells. *Cell Mol Bioeng*. 2009;2(3):332-340.
18. Chevrier A, Nelea M, Hurtig MB, Hoemann CD, Buschmann MD. Meniscus structure in human, sheep, and rabbit for animal models of meniscus repair. *J Orthop Res*. 2009;27(9):1197-1203.
19. Gray JC. Neural and vascular anatomy of the menisci of the human knee. *J Orthop Sports Phys Ther*. 1999;29(1):23-30. doi:10.2519/jospt.1999.29.1.23
20. Kestilä I, Folkesson E, Finnilä MA, et al. Three-dimensional microstructure of human meniscus posterior horn in health and osteoarthritis. *Osteoarthritis Cartilage*. 2019;27(12):1790-1799.
21. Karjalainen V-P, Kestilä I, Finnilä MA, et al. Quantitative three-dimensional collagen orientation analysis of human meniscus posterior horn in health and osteoarthritis using micro-computed tomography. *Osteoarthritis Cartilage*. 2021;29(5):762-772.
22. Englund M, Roos EM, Lohmander LS. Impact of type of meniscal tear on radiographic and symptomatic knee osteoarthritis: a sixteen-year followup of meniscectomy with matched controls. *Arthritis Rheum*. 2003;48(8):2178-2187.
23. Canciani B, Herrera Millar VR, Pallaoro M, et al. Testing hypoxia in pig meniscal culture: biological role of the vascular-related factors in the differentiation and viability of neonatal meniscus. *Int J Mol Sci*. 2021;22(22):12465.
24. Hellberg I, Karjalainen VP, Finnilä MAJ, et al. 3D analysis and grading of calcifications from ex vivo human meniscus. *Osteoarthritis Cartilage*. 2023;31(4):482-492.
25. Di Giancamillo A, Deponti D, Modena S, Tessaro I, Domeneghini C, Peretti GM. Age-related modulation of angiogenesis-regulating factors in the swine meniscus. *J Cell Mol Med*. 2017;21(11):3066-3075.
26. Di Giancamillo A, Deponti D, Addis A, Domeneghini C, Peretti GM. Meniscus maturation in the swine model: changes occurring along with anterior to posterior and medial to lateral aspect during growth. *J Cell Mol Med*. 2014;18(10):1964-1974.
27. Aidos L, Modena SC, Millar VRH, et al. Meniscus matrix structural and biomechanical evaluation: age-dependent properties in a swine model. *Bioengineering*. 2022;9(3):117.
28. Petersen W, Tillmann B. Age-related blood and lymph supply of the knee menisci. A cadaver study. *Acta Orthop Scand*. 1995;66(4):308-312.
29. Tsujii A, Nakamura N, Horibe S. Age-related changes in the knee meniscus. *Knee*. 2017;24(6):1262-1270.
30. Bray RC, Smith JA, Eng MK, Leonard CA, Sutherland CA, Salo PT. Vascular response of the meniscus to injury: effects of immobilization. *J Orthop Res*. 2001;19(3):384-390.
31. Ashraf S, Wibberley H, Mapp PI, Hill R, Wilson D, Walsh DA. Increased vascular penetration and nerve growth in the meniscus: a potential source of pain in osteoarthritis. *Ann Rheum Dis*. 2011;70(3):523-529.
32. Sosio C, Di Giancamillo A, Deponti D, et al. Osteochondral repair by a novel interconnecting collagen-hydroxyapatite substitute: a large-animal study. *Tissue Eng Part A*. 2015;21(3-4):704-715. <https://home.liebertpub.com/tea>
33. Mapp PI, Walsh DA. Mechanisms and targets of angiogenesis and nerve growth in osteoarthritis. *Nat Rev Rheumatol*. 2012;8(7):390-398. <https://www.nature.com/articles/nrrheum.2012.80>
34. Pauli C, Grogan SP, Patil S, et al. Macroscopic and histopathologic analysis of human knee menisci in aging and osteoarthritis. *Osteoarthritis Cartilage*. 2011;19(9):1132-1141.
35. Patel JM, Saleh KS, Burdick JA, Mauck RL. Bioactive factors for cartilage repair and regeneration: improving delivery, retention, and activity. *Acta Biomater*. 2019;93:222-238.
36. Toms AP, White LM, Marshall TJ, Donell ST. Imaging the post-operative meniscus. *Eur J Radiol*. 2005;54(2):189-198.
37. Brindle T, Nyland J, Johnson DL. The meniscus: review of basic principles with application to surgery and rehabilitation. *J Athl Train*. 2001;36(2):160-169.
38. Arnoczky SP. Gross and vascular anatomy of the meniscus and its role in meniscal healing, regeneration and remodeling. In: Mow VC, Arnoczky SP, Jackson SW, eds. *Knee Meniscus: Basic and Clinical Foundations*. Raven Press; 1992:1-14.
39. Fox AJS, Bedi A, Rodeo SA. The basic science of human knee menisci. *Sports Health*. 2012;4(4):340-351.
40. Herrera Millar VR, Canciani B, Mangiavini L, et al. Endostatin in 3D fibrin hydrogel scaffolds promotes chondrogenic differentiation in swine neonatal meniscal cells. *Biomedicine*. 2022;10(10):2415.

41. Wang H, Chen T, Torzilli P, Warren R, Maher S. Dynamic contact stress patterns on the tibial plateaus during simulated gait: a novel application of normalized cross correlation. *J Biomech.* 2014;47(2):568-574.
42. Makris EA, Hadidi P, Athanasiou KA. The knee meniscus: structure–function, pathophysiology, current repair techniques, and prospects for regeneration. *Biomaterials.* 2011;32(30):7411-7431.
43. Sweigart MA, Zhu CF, Burt DM, et al. Intraspecies and interspecies comparison of the compressive properties of the medial meniscus. *Ann Biomed Eng.* 2004;32(11):1569-1579. <https://link.springer.com/article/10.1114/B:ABME.0000049040.70767.5c>
44. Bansal S, Floyd ER, A Kowalski M, et al. Meniscal repair: the current state and recent advances in augmentation. *J Orthop Res.* 2021;39(7):1368-1382.
45. Li H, Li P, Yang Z, et al. Meniscal regenerative scaffolds based on biopolymers and polymers: recent status and applications. *Front Cell Dev Biol.* 2021;9:661802.
46. Joshi MD, Suh JK, Marui T, Woo SLY. Interspecies variation of compressive biomechanical properties of the meniscus. *J Biomed Mater Res.* 1995;29(7):823-828.
47. Abdelgaied A, Stanley M, Galfe M, Berry H, Ingham E, Fisher J. Comparison of the biomechanical tensile and compressive properties of decellularised and natural porcine meniscus. *J Biomech.* 2015;48(8):1389-1396.
48. Sweigart MA, Athanasiou KA. Biomechanical characteristics of the normal medial and lateral porcine knee menisci. *Proc Inst Mech Eng Part H.* 2005;219(1):53-62. <https://journals.sagepub.com/doi/abs/10.1243/095441105X9174?journalCode=pihb>
49. Natsuyama Y, Zhang M, Yang T, et al. Morphological study of the arterial supply to the menisci in pigs with special reference to creating meniscus injury model. *Folia Morphol (Warsz).* Published online June 7, 2023. [doi:10.5603/FM.a2023.0041](https://doi.org/10.5603/FM.a2023.0041)
50. Peretti GM, Polito U, Di Giancamillo M, et al. Swine meniscus: are femoral-tibial surfaces properly tuned to bear the forces exerted on the tissue? *Tissue Eng Part A.* 2021;25(13-14):978-989.
51. Ludin A, Sela JJ, Schroeder A, Samuni Y, Nitzan DW, Amir G. Injection of vascular endothelial growth factor into knee joints induces osteoarthritis in mice. *Osteoarthritis Cartilage.* 2013;21(3):491-497.
52. Katsamenis OL, Karoutsos V, Kontostanos K, et al. Microstructural characterization of CPPD and hydroxyapatite crystal depositions on human menisci. *Cryst Res Technol.* 2012;47(11):1201-1209. <https://onlinelibrary.wiley.com/doi/full/10.1002/crat.201200346>
53. Yavorsky A, Hernandez-Santana A, McCarthy G, McMahon G. Detection of calcium phosphate crystals in the joint fluid of patients with osteoarthritis – analytical approaches and challenges. *Analyst.* 2008;133(3):302-318. <https://pubs.rsc.org/en/content/articlehtml/2008/an/b716791a>
54. Englund M, Guermazi A, Gale D, et al. Incidental meniscal findings on knee MRI in middle-aged and elderly persons. *N Engl J Med.* 2008;359(11):1108-1115.
55. Ford GM, Hegmann KT, White GL, Holmes EB. Associations of body mass index with meniscal tears. *Am J Prev Med.* 2005;28(4):364-368.
56. van der Voet JA, Runhaar J, van der Plas P, Vroegindewij D, Oei EH, Bierma-Zeinstra SMA. Baseline meniscal extrusion associated with incident knee osteoarthritis after 30 months in overweight and obese women. *Osteoarthritis Cartilage.* 2017;25(8):1299-1303.
57. Bendele AM, Hulman JF. Effects of body weight restriction on the development and progression of spontaneous osteoarthritis in Guinea pigs. *Arthritis Rheum.* 1991;34(9):1180-1184.
58. Achtnich A, Petersen W, Willinger L, et al. Medial meniscus extrusion increases with age and BMI and is depending on different loading conditions. *Knee Surg Sports Traumatol Arthrosc.* 2018;26(8):2282-2288.
59. Nation JL. A new method using hexamethyldisilazane for preparation of soft insect tissues for scanning electron microscopy. *Stain Technol.* 1983;58(6):347-351.
60. Klinger P, Surmann-Schmitt C, Brem M, et al. Chondromodulin 1 stabilizes the chondrocyte phenotype and inhibits endochondral ossification of porcine cartilage repair tissue. *Arthritis Rheum.* 2011;63(9):2721-2731.

SUPPORTING INFORMATION

Additional supporting information can be found online in the Supporting Information section at the end of this article.

How to cite this article: Karjalainen V-P, Herrera Millar VR, Modina S, et al. Age and anatomical region-related differences in vascularization of the porcine meniscus using microcomputed tomography imaging. *J Orthop Res.* 2024;1-11. [doi:10.1002/jor.25862](https://doi.org/10.1002/jor.25862)